The Muenster Redshift Project. Automated Redshift Measurements from Low-Dispersion Objective Prism Schmidt Plates

P. Schuecker
Astronomisches Institut
Westfälische Wilhelms-Universität
Münster, F.R. Germany

Abstract

A three-dimensional galaxy survey at faint magnitudes and over large volumes of space is currently carried out at Muenster. In order to enhance the reliability of the redshifts measured from objective prism plates, three different methods are used: the *correlation method*, the *least-squares method* and the *break method* where continuum breaks are identified directly. The redshift errors of the individual methods are $dz = 0.007$ (correlation), 0.011 (direct identification) and 0.016 (least-squares). In the majority of cases two *independent* measurements are possible leading to mean redshift values with errors of 0.008. To date redshifts of 24 000 galaxies with $17^{\rm m} < {\rm m_J} < 20^{\rm m}$ have been obtained. The current rate is an increase of 6 000 galaxy redshifts per measuring week.

1 Introduction

In 1986 the Astronomical Institute Muenster (AIM) has started a three-dimensional redshift survey, the Muenster Redshift Project (MRSP). A major goal of MRSP is to study the complex structures of clusters and superclusters of galaxies on large scales, *i.e.* in large solid angles and up to at least $0.3\,c$. The observational data are obtained from direct and objective prism Schmidt plates. The direct plates are used for the identification of galaxies and clusters of galaxies, the very low dispersion objective prism plates for measuring galaxy positions in redshift space. From these positions the locations of galaxies in the depth of real space and information about their membership in clusters and superclusters are obtained.

All plates are digitized with the PDS 2020 GMplus and processed fully automatically with the software system ADAS (Astronomical Data Analysing System, ADAS 1987) of AIM (Teuber 1988). MRSP provides galaxy positions with accuracies of about $0''.4$ (Tucholke 1988), galaxy magnitudes $16^{\rm m}.5 \leq {\rm m_J} \leq 21^{\rm m}.5$ with accuracies $0^{\rm m}.1$ (Horstmann 1988) and redshifts $0 \leq z \leq 0.3$ with an average accuracy ≤ 0.008 in the range $17^{\rm m} < {\rm m_J} < 20^{\rm m}$. One plate covers 30 square degrees and includes about 40 000 galaxies in fields near the South Galactic Pole. Typical subsamples of galaxies contain 25 000 galaxies with rough *morphological types* from the direct Schmidt plate and 6 000 galaxies with *redshifts* from the objective prism plate. For one objective prism plate the total reduction time is one week.

In the present paper three methods for automated redshift measurements are discussed. In Sect. 2 the reduction of the spectra prior to redshift determination is introduced. Sect. 3 describes the three methods of automated redshift determination. Sect. 4 contains the error estimates and Sect. 5 the conclusions and future plans.

2 Reduction of the objective prism spectra

2.1 Spectral features at low dispersions

Studies concerning the determination of radial velocities of faint galaxies from Curtis and UK Schmidt telescope plates by Cooke *et al.* (1977, 1981) show the possibility of determining galaxy redshifts using very low dispersions (140 and 246 nm mm^{-1} at Hγ). In these cases, however, radial velocities cannot be determined by measuring line positions: the size of the seeing disc during exposure and the effective angular size of the galaxy limit the spectral resolution and smear out all smaller spectral features. The only features seen in the galaxy spectra up to redshifts 0.3 on IIIa-J plates with a dispersion 246 nm mm^{-1} at Hγ are

- a strong absorption feature at 400 nm (400 nm break), mainly caused by the blend of Ca II H, K with contributions of Hϵ and metallic blends. This is the most prominent spectral feature.
- a feature at 430 nm (430 nm break) corresponding to the G-band with Hγ and metallic blends, enhanced by an emulsion dip
- a weak absorption feature at 365 nm caused by Fe I blends.

Simulations with model spectra of Kurucz (1979) show that weak absorption systems of Fe II 233–263 nm and Mg II 280 nm can be used in galaxy spectra with $0.3 < z < 1.0$ (Schuecker 1986a).

Redshifts from objective prism spectra are obtained by measuring the distances between the breaks and a suitably chosen reference point. Beard *et al.* (1986) and Parker *et al.* (1987) used the position of the emulsion cutoff of the J-emulsion near 538 nm. In the present investigation a zero point transformation from the direct plate is employed (see Sect. 2.4).

So far, one major problem in obtaining large numbers of galaxy redshifts is the time consuming *interactive* measuring process. Some investigations toward automatization are given in Cooke *et al.* (1983, 1984) and Bunclark (1984). In the present communication various methods of *automated* redshift measurements from low-dispersion spectra are introduced. The observational material consists of film copies of unfiltered IIIa-J objective prism plates with a dispersion of 246 nm mm^{-1} at Hγ taken with the UK Schmidt telescope and prism 1. Each plate covers 41 square degrees of which 23 square degrees are nominally unvignetted. The limiting magnitude is $m_J = 20^{\mathrm{m}}.5$ (Tritton 1983).

2.2 Digitization and automated detection of objective prism spectra

Film copies from direct UK Schmidt plates as distributed in the ESO/SRC Atlas and copies of the corresponding UK objective prism plates are digitized with the microdensitometer PDS 2020 GMplus of AIM with step size 15 μm, aperture 20 $\times$ 20 μm^2, and density range 0.0 – 4.5. After *segmentation* of the objective prism plate (Horstmann 1988) the spectra of all objects brighter than $20^{m}.5$ on the direct plate, *e.g.* 50 000 spectra in high galactic latitude fields, 35 000 of starlike objects and 15 000 of galaxies, are stored for further processing. Each spectrum is represented by an arrray of 101 $\times$ 15 pixels. In addition, information is given about the position of the object, the positions of its nearest neighbours and their apparent magnitudes, object type (star or galaxy as classified on the direct plate), object size and shape, and the local sky background and background noise. The information about the nearest neighbours is used to identify overlapping spectra.

2.3 Preprocessing of the spectra

The density of each pixel in the stored spectrum array is transformed into a relative intensity I_{ij} using the step wedges given on the UKST plates. The spectral profile I_i (*Fig. 1*) is obtained from marginal sums perpendicular to the direction of dispersion, where each pixel I_{ij} is weighted according to a mean intensity distribution function DF_j. Unlike the point spread function, the DF_j for extended objects comprises both the distortions along the light path and the effects of light distribution over the extended image. It is thus essential that the DF_j is determined individually for each object. The DF_j is estimated from the marginal sums in the direction of dispersion, and normalized to values between 0 and 1 (i: in the direction of dispersion, j: perpendicular to i):

$$I_i = \frac{\sum_j I_{ij} DF_j}{\sum_j DF_j} \tag{1}$$

with

$$DF_j = \frac{\Phi_j - \Phi_{min}}{\Phi_{max} - \Phi_{min}}, \quad \Phi_j = \sum_i I_{ij} \; .$$

Rebinning of the pixel coordinates x, represented in Eqn. 1 by the discrete coordinates i, into other coordinates λ, *e.g.* wavelengths, leads to corrections of the intensities which are large in the case of large nonlinear terms in the transformation curve $\lambda(x)$:

$$I(\lambda) = I(x) \left[\frac{\partial \lambda(x)}{\partial x} \right]^{-1} \; . \tag{2}$$

The transformation of the plate scale x into a wavelength $\lambda(x)$ or a logarithmic wavelength scale uses the dispersion curve of the prism. For prism 1 of the UKST the dispersion curve was determined by Nandy *et al.* (1977). The final rebinning is computed with cubic spline interpolations. The nonlinear transformation (Eqn. 2) leads to a wavelength dependence of the noise and a (partial) restauration of the spectral features on the linear wavelength scale.

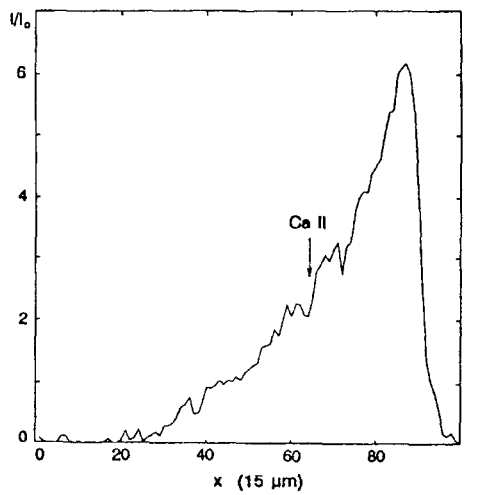

Fig. 1. Intensity profile of a low-dispersion objective prism galaxy spectrum.

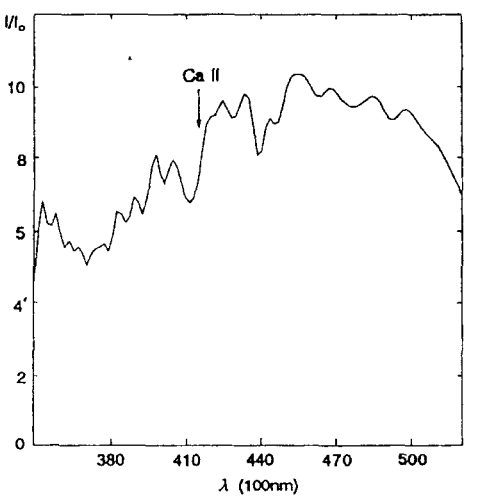

Fig. 2. Intensity profile of *Fig. 1* corrected for atmospheric extinction, transmission of the prism and the achromatic correcting plate and the sensitivity of the emulsion.

Intensity profiles corrected for atmospheric extinction $E(\lambda)$, transmission of the prism $P(\lambda)$ and the achromatic correcting plate $A(\lambda)$, and the sensitivity of the emulsion $S(\lambda)$ are needed for some purposes, *e.g.* for the calculation of equivalent widths in emission line objects and for galaxy redshift measurements by least-squares comparisons of spectral profiles. Corrected profiles (*Fig. 2*) are obtained from Eqn. 3, the filter functions are taken from Clowes *et al.* (1980):

$$I(\lambda)_{corr} = I(\lambda)\,[E(\lambda)\,P(\lambda)\,A(\lambda)\,S(\lambda)]^{-1}\ . \tag{3}$$

2.4 The wavelength reference point

A critical process for reliable wavelength measurements is the determination of the wavelength reference point. Emerson (1981, 1983) and Beard *et al.* (1986) showed that the frequently used emulsion cutoff introduces a systematic error $\leq 50\,\mu$m depending on magnitude and colour of the object. This leads to radial velocity errors from $\leq 6\,600$ km s^{-1} at 400 nm to $\leq 11\,500$ km s^{-1} above 500 nm.

The MRSP uses the transformation from direct plate positions of automatically selected G-type stars to the positions of their 400 nm breaks on the objective prism plate. The error obtained in x is $0''.33$, corresponding to 700 km s^{-1} at $z = 0.0$ and 1 200 km s^{-1} at $z = 0.3$. This is the limit of the redshift accuracy attainable. More information about the wavelength calibration is given by Tucholke *et al.* (1988) and Tucholke (1988).

Details about the automated classification, especially for M- and G-type stars, are given by Schuecker (1986b) and Schuecker *et al.* (1986, 1988a). The classification will be extended to all MK-spectral classes using low-dispersion classification criteria given by Seitter (1988).

2.5 Rectification

2.5.1 About the use of fuzzy algebra

A basic problem in automated redshift measurement is the correct identification of the chosen spectral feature. In order to make such a feature visible at low dispersions, it is essential that a suitable reference continuum is defined. Usual methods, like polynomial fits *etc.*, fix the continuum with regard to *one* criterion only. In order to get solutions which optimize *several* criteria, *fuzzy algebra* is applied.

In a fuzzy set C the transition from membership to nonmembership is continuous and for any point characterized by a declining sequence of numbers μ_C (Zadeh 1965). C is defined as a set of n pairs

$$C = \{(\mu_C(L_i),\, L_i);\quad i = 1, 2, \ldots, n\}\ . \tag{4}$$

For each point L_i, $\mu_C(L_i)$ gives the degree of membership in C. Therefore, C includes the concept of ordinary sets if $\mu_C = 0$ or 1. A standard expression of the membership function $\mu_C(L)$ is the S-function (Zadeh 1975):

$$S(L; a, b, c) = \begin{cases} 0 & a > L \\ 2(\frac{L-a}{c-a})^2 & a \leq L < b \\ 1 - 2(\frac{L-c}{c-a})^2 & b \leq L \leq c \\ 1 & c < L \end{cases} \qquad c \neq a \neq 0 \tag{5}$$

with

$$b = \frac{a+c}{2}\ .$$

It is an S-shaped function with the parameters a, b, c where b determines the cross-over point. S- or other membership functions are similar to probability distribution

functions, but conceptually different (Pal and Dutta Majumder 1986): while the probability distribution function describes how *frequently* values $\leq L$ occur, the membership function indicates how *closely* L resembles an ideal element. The choice of the function for the solution of a special problem is *ad hoc* and only based on the fact that it gives useful results. The unique evaluation of membership functions is a ongoing major controversy in fuzzy set theory.

The intersection between different fuzzy sets C_i is calculated from the values of the contributing membership functions (Zadeh 1965, 1968, 1973):

$$\mu_{intersection}(L) = \min_L\{\mu_{C_1}(L), \mu_{C_2}(L), \ldots\} \; . \tag{6}$$

Weighting of the different sets is attainable *e.g.* with exponential fuzzifiers e:

$$\mu_{weighted}(L) = [\mu(L)]^e \; . \tag{7}$$

They also offer the possibility to modify the slope of the membership function.

2.5.2 Rectification with fuzzy algebra

In terms of fuzzy sets, the problem of rectification can be formulated as follows. Given is a set of different reference continua $\{R_i^L\}$ with parameter L. L, *e.g.* the filter width, is chosen for the calculation of the different continua. The problem is to find the continuum (*i.e.* the value of L) which optimizes the criteria and thus yields the properties of the wanted continuum. Each criterion must be represented by a fuzzy set. The intersection of the different fuzzy sets (Eqn. 6) represents the combination of the different criteria. The value L with the highest membership gives the continuum which satisfies all criteria *best*. The criteria chosen here are:

1: clear protrusion of breaks above the reference continuum

2: smoothness of the continuum (short length)

3: good approximation of the spectrum (low *rms*).

The different reference continua R_i^L are computed by cubic spline interpolations between k knots selected from the intensity profile I_i. The knots are defined by the minima found in k wavelength intervals of I_i. The parameter L is the length of the interval. For low values of L the approximation of I_i increases, whereas the smoothness of the continuum and the protrusion of the breaks decrease. For large L the breaks are more clearly visible but the approximation of I_i decreases.

The three criteria constitute three fuzzy sets. To evaluate the corresponding membership functions, *e.g.* the parameters a, b, c of the S-function (Eqn. 5), the criteria are given in quantitative forms:

$$\begin{aligned} &\text{Criterion 1:} \quad \max \delta_L = \textstyle\sum_i (I_i - R_i^L) \\ &\text{Criterion 2:} \quad \min \theta_L = \textstyle\sum_i \sqrt{1 + \left(\frac{\partial R_i^L(\lambda)}{\partial \log \lambda}\right)^2} \\ &\text{Criterion 3:} \quad \min \epsilon_L = \textstyle\sum_i (I_i - R_i^L)^2 \end{aligned} \tag{8}$$

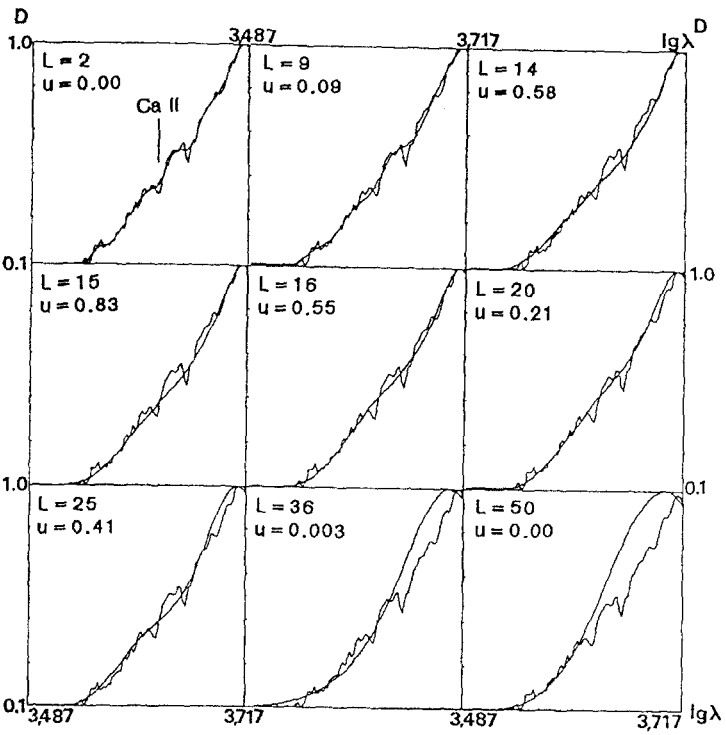

Fig. 3. Reference continua superimposed on a galaxy spectrum profile. L is the parameter of the reference continuum, μ is the membership value of the intersecting fuzzy set. The chosen reference continuum has the hightest membership value $\mu = 0.83$ and $L = 15$.

The quantities δ_L, θ_L and ϵ_L are calculated for each reference continuum R_i^L. Physically meaningful values of L lead to sets $\{\delta_L\}$, $\{\theta_L\}$ and $\{\epsilon_L\}$, from which convenient membership functions can be obtained. If the S-function is used, the extrema of δ_L, θ_L and ϵ_L define the parameters a, b, c:

$$\begin{array}{lll} a_\delta = \min_L\{\delta_L\} & c_\delta = \max_L\{\delta_L\} & b_\delta = \frac{a_\delta + c_\delta}{2} \\ a_\theta = \min_L\{\theta_L\} & c_\theta = \max_L\{\theta_L\} & \ldots \\ a_\epsilon = \min_L\{\epsilon_L\} & c_\epsilon = \max_L\{\epsilon_L\} & \ldots \end{array} \tag{9}$$

The corresponding membership functions are:

$$\begin{aligned} \mu_\delta(L) &= \{\quad S(L; a_\delta, b_\delta, c_\delta)\ \}^{e_1} \\ \mu_\theta(L) &= \{1 - S(L; a_\theta, b_\theta, c_\theta)\ \}^{e_2} \\ \mu_\epsilon(L) &= \{1 - S(L; a_\epsilon, b_\epsilon, c_\epsilon)\ \}^{e_3} \end{aligned} \tag{10}$$

with the exponential fuzzifiers e_1, e_2 and e_3. $\mu_\delta = 1$ corresponds to a continuum showing the breaks in the spectrum I_i best. $\mu_\delta = 0$ is the membership value for the continuum with the worst representation of the breaks. Corresponding relations hold for μ_θ and μ_ϵ. Eqn. 6 gives the intersection of the fuzzy sets. The value L with the highest membership of the resulting fuzzy set yields the wanted reference continuum.

Figure 3 shows reference continua with different search intervals L for a galaxy spectrum (type Sc, $m_J = 16^{\mathrm{m}}.3$). They are chosen from a total of 49 different continua. L varies between $L = 2$ ($d\log\lambda = 0.0046$) and $L = 50$ (0.115). The adjusted values for the exponential fuzzifiers are $e_1 = 10.0$, $e_2 = 1.0$ and $e_3 = 0.1$. Membership values from Eqn. 6 lie between $\mu = 0.00$ and $\mu = 0.83$. Curves with $\mu = 0.00$ represent continua where one or more criteria completely fail: for $L = 2$ and 50 no clear protrusion of the 400 nm break is achieved. In addition, the continuum for $LL = 2$ is rather long. The *best* reference continuum has $L = 15$.

The different S/N ratios of the galaxies lead to different values of L for the optimal reference continua. Therefore, the procedure described above must be applied individually to each spectrum.

3 Methods for redshift determination

3.1 The correlation method

After rebinning the x-scales of the spectra into logarithmic wavelength scales (Eqn. 2), redshifts correspond to uniform linear shifts of the spectral features. In order to find the redshift z of a galaxy spectrum I_i, one has to find the template spectrum T_i^z most similar to I_i from a set of templates with known redshifts $\{T_i^z\}$. This is performed with the generalized correlation function (*e.g.* Bracewell 1978):

$$c_z = \frac{\sum_i I_i T_i^z}{\sqrt{\sum_i (I_i)^2 \sum_i (T_i^z)^2}} \,. \tag{11}$$

The normalization factor leads to correlations c_z between -1 (anticorrelation) and $+1$ (ideal correlation, autocorrelation). The template T_i^z which maximizes c_z is the chosen template. The position of the correlation peak gives the redshift of the programme galaxy.

Figure 4 presents correlation functions between a G-type star template and three galaxy spectra. The correct redshifts of the galaxy spectra, taken from Parker *et al.* (1986) and West and Frandsen (1981), are indicated by arrows. A G-type star template was chosen because most of the integral galaxy spectra are of this spectral type (Humason *et al.* 1956). The set of templates $\{T_i^z\}$ is created by artificially shifting the G-type spectrum relative to the galaxy spectrum.

The correlation is more sensitive to redshift when rectified spectra with their continua subtracted are matched. This mode was used here. For rectification the procedure outlined in Sect. 2.5 is applied. In order to measure redshifts up to twice as large as those obtained by using periodic boundary conditions (*e.g.* FFT, Simkin 1974) zeros are appended to both ends of the spectra. Larger shifts between T_i^z and I_i lead, however, to lower numbers of spectrum pixels available for the calculation of the cross term in Eqn. 11. Therefore, correlation peaks at large shifts have lower weight than peaks at small shifts.

In *Fig. 4a* the position of the highest correlation peak gives the correct redshift. The neighbouring peaks correspond to the 430 nm breaks. *Figs. 4b* and *c* illustrate two

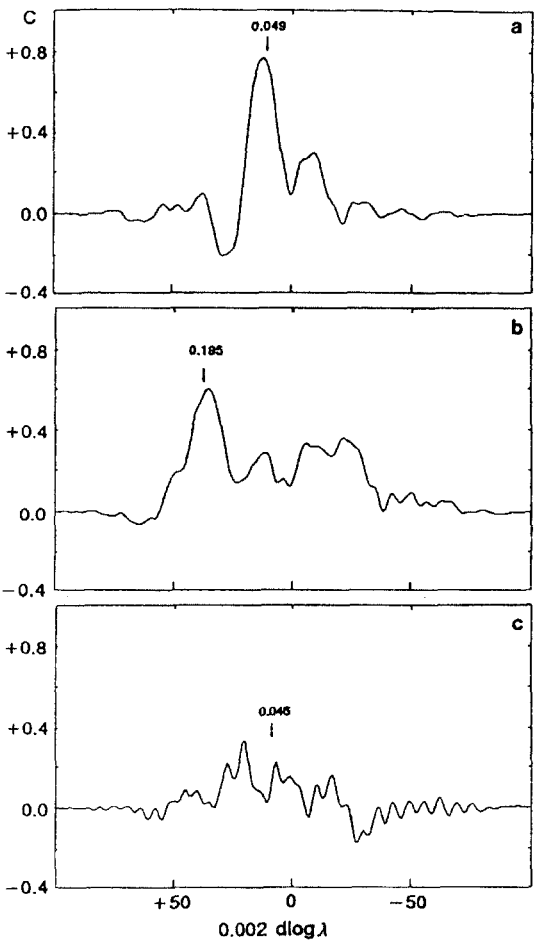

Fig. 4. Correlation functions c between a G-type star template and three galaxy spectra. The correct redshifts are indicated by arrows.
4a: The position of the highest correlation peak gives the correct redshift.
4b: Correlation function with local registration error.
4c: Correlation function with false acquisition error.

important correlation errors (Ryan and Hunt 1981):

- *Local registration errors* occur when the breaks are smeared out, resulting in broader correlation peaks with shifted maximum positions (*Fig. 4b*). The distortions of the breaks are caused by seeing effects and grain noise of the emulsion. Because of the highly nonlinear dispersion curve of the prism, local registration errors are larger in the red spectral range. Estimates of the correlation errors, *e.g.* from the asymmetric component of c_z (Tonry and Davis 1979), are thus dependent on wavelength, *i.e.* redshift, and cannot be computed with simple analytic expressions.

- *False acquisition errors* occur when different breaks or large noise peaks in the spectra

lead to more than one prominent correlation peak. The position of the highest peak may not give the correct redshift (*Fig. 4c*). In contrast to local registration errors, which are more or less random, false acquisition errors can lead to large systematic redshift errors. To circumvent this, additional methods for redshift measurements must be applied. They determine the *redshift range* in the correlation function where the correct correlation peak is expected. Two such methods are given in the following sections.

Details about the redshift accuracy attainable with the correlation method are given in Sect. 4.

3.2 The least-squares method

The method of measuring redshifts by comparing intensity distributions of galaxies of unknown redshifts with those of known redshifts was originally developed by Baum (1962). In order to measure the redshifts of clusters of galaxies, he averaged multicolour photometric intensities of galaxies in each cluster, thus increasing the S/N ratios of the distributions, and compared the intensity distributions to those of galaxies with known redshifts. Oke (1971) improved this observational procedure and was able to compare the photometric data of *individual* galaxies with suitable templates. More recent work using the photometric redshift method is reported by Loh (1988).

A corresponding method can also be used with spectra. It is to find the *best* template T_i^z which leads to a minimum sum of (unweighted) squared deviations between the actual programme spectrum I_i and the different templates T_i^z:

$$s_z^2 = \sum_i (I_i - T_i^z)^2 \,. \tag{12}$$

In most cases the S/N ratios of individual programme galaxy spectra are low. If the S/N ratios of the templates are also low, s_z^2 is dominated by noise and therefore not sensitive to redshift. To reduce this problem, templates with high S/N ratios should be used.

For measuring redshifts from objective prism spectra with this method, intensity profiles corrected with Eqn. 3 are compared. The profiles are normalized to equal intensities at 520 nm. The templates $\{T_i^z\}$ are created by shifting one template along the logarithmic wavelength axis to artificial redshifts. As in the case of template matching via correlations, the programme spectrum has to be extended on both sides, here using the mean intensities at the beginning and at the end of the spectra. The template which minimizes Eqn. 12 determines the redshift.

Figure 5 gives three cases of s^2-values vs. differences in logarithmic wavelengths between the programme galaxies and a G-type star. *Fig. 5a* illustrates a correct least-squares mininum. *Fig. 5b* and *c* show errors analogous to the local registration and false acquisition errors (Sect. 3.1). The fact that the same types of errors occur in both methods relies on similarities between *least-squares minimization* and *correlation maximization* as shown by Ryan and Hunt (1981).

In contrast to the correlation method where rectified spectra are compared, the least-

squares method is perfomed with intensity profiles, including both the line spectra and continua. While the correlation method is more sensitive to redshift, resulting in sharp peaks of the correlation function, the advantage of the smoother least-squares curves is that the effects of noise or other spurious features are suppressed. Here the possible *systematic errors* mentioned above are more clearly visible.

Another important redshift error of both methods is caused by different intrinsic colours of galaxies. To reduce this error, template galaxies (or artificially redshifted stars) of different spectral types must be used.

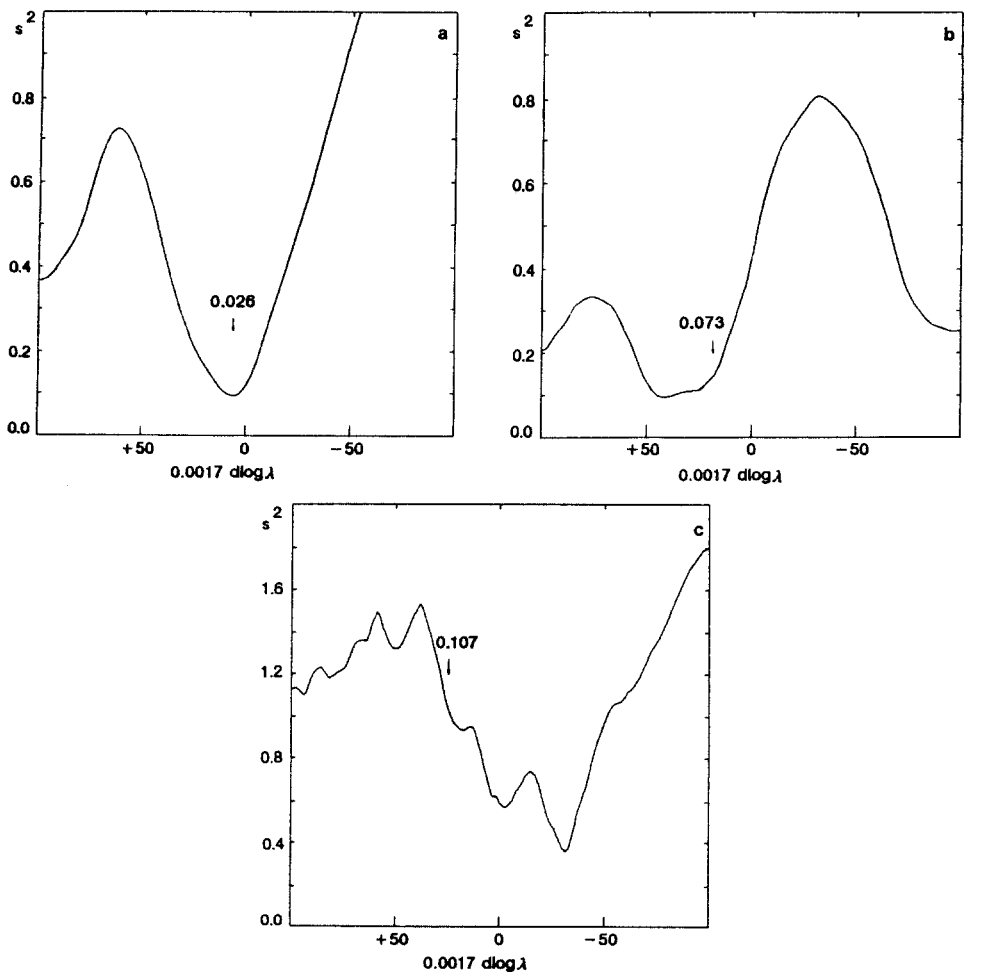

Fig. 5. Least-squares functions s^2 between a G-type star template and three galaxy spectra. The correct redshifts are indicated by arrows.
5a: The position of the s^2-minimum gives the correct redshift.
5b: s^2-function with local registration error.
5c: s^2-function with false acquisition error.

3.3 The break measuring method

The two methods described in Sects. 3.1 and 3.2 give integral measures of the galaxy redshifts. They use all spectral features without identifying them individually. In this section a method for the automated identification of breaks is described.

3.3.1 Search for individual breaks

From Eqn. 2 it is apparent that the nonlinear dispersion curve of the prism affects the intensity profiles of all spectra in a characteristic way: the spectral intensities increase with increasing wavelengths. Thus, strong absorption systems have depressed intensities at their short wavelength end, leading to a break-like appearence. This suggests the following break detection method:

At a certain number of pre-determined intensity levels of an intensity profile $I(\lambda)$ the corresponding wavelengths are determined. Several neighbouring intensity values found within a small wavelength interval indicate the presence of a break. The combination of numbers of intensity levels and width of the wavelength interval must satisfy preset criteria. These given, the wavelength groups are found by *cluster analysis.*

3.3.2 Identification of breaks

Spectrum profiles with different numbers of breaks are given in *Fig. 6.* For a one break spectrum it is always assumed that the detected feature is the strongest one, *i.e.* the 400 nm break. A two break spectrum is most likely to show the 400 nm and the 430 nm break, the two most prominent features in a galaxy spectrum. In order to ensure correct identifications, the two detected breaks must give similar redshifts. Spectra of this kind are found for galaxies with redshifts $z < 0.25$; at higher redshifts the 430 nm break is not observable on the IIIaJ-emulsion used.

Spectra with no break are frequently overexposed and thus rejected. Peculiar galaxy profiles may have more than two prominent breaks. For faint spectra it is expected that some of them show the Mg II or Fe II absorptions, indicating large redshifts and extremly high absolute luminosities. A special study of those objects is in preparation.

After identification of the breaks the final redshift is obtained by measuring the position of half maximum intensity of the 400 nm break using polynomial fits. Additional fits to the 430 nm break, when present, are not necessary because the position of this break is not as well determined as that of the 400 nm break, leading to higher redshift errors.

4 Estimates of redshift accuracies

The redshift accuracies for the three methods described in Sect. 3 are discussed here. Because of the small number of galaxy redshifts obtained from slit spectra in the relevant magnitude and redshift ranges ($17^{\mathrm{m}}.0 < m_J < 20^{\mathrm{m}}$; $z \leq 0.3$) the redshift accuracies are estimated by comparing the redshifts measured with the individual methods. The redshifts are obtained for SRC field No. 411. In the following the sub-

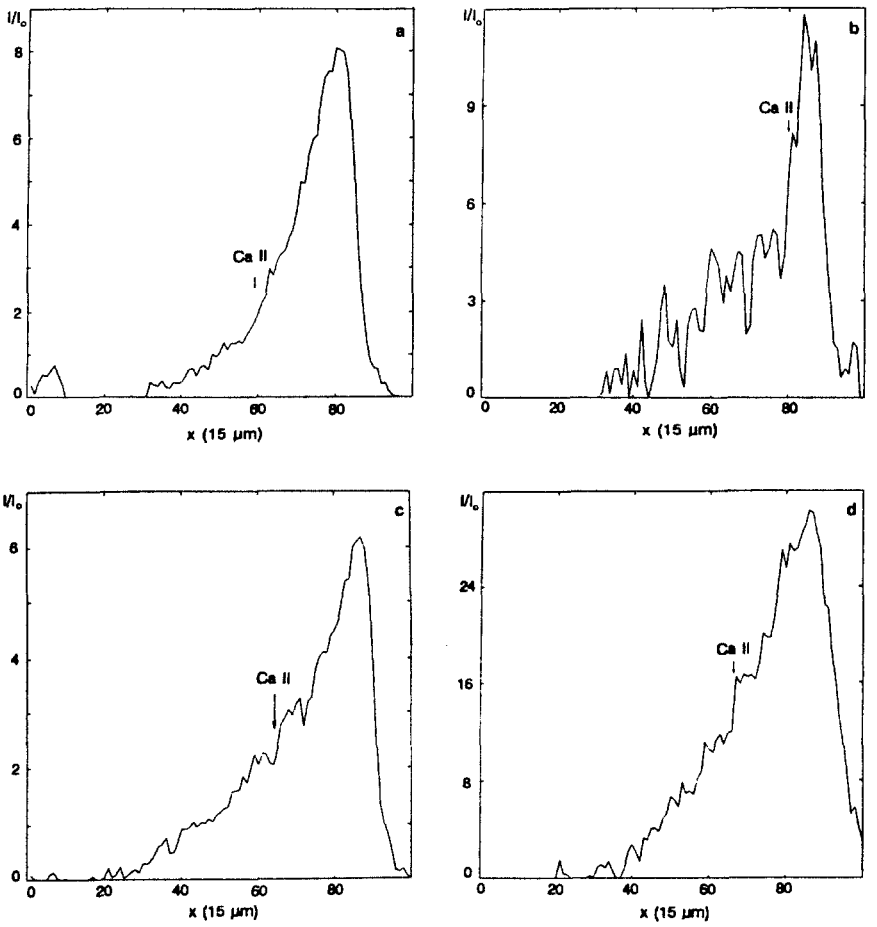

Fig. 6. Galaxy spectrum profiles with
6a: no break, 6b: one break, 6c: two breaks, 6d: three breaks.

script 'C' denotes *correlation method* (Sect. 3.1), 'L' *least-squares method* (Sect. 3.2) and 'B' *break measuring method* (Sect. 3.3)

4.1 Systematic errors

In the first step *systematic errors* are detected and corrected. For this the redshifts z_L and z_B are compared. One break galaxies are plotted in *Fig. 7a*, two break galaxies in *Fig. 7b*. In contrast to one break galaxies, two break galaxies might have z_L redshifts with false acquisition errors, the minima of the s^2-relation are caused by the 430 nm break and not by the 400 nm break. Galaxy redshifts with this error are located in a region nearly parallel to the diagonal in *Fig. 7b*. *Fig. 7c* shows the relation between redshifts *after correcting* z_L for the false acquisition error. Galaxies are rejected when large redshift differences $z_L - z_B$ are found which cannot be explained by systematic confusions of spectral features.

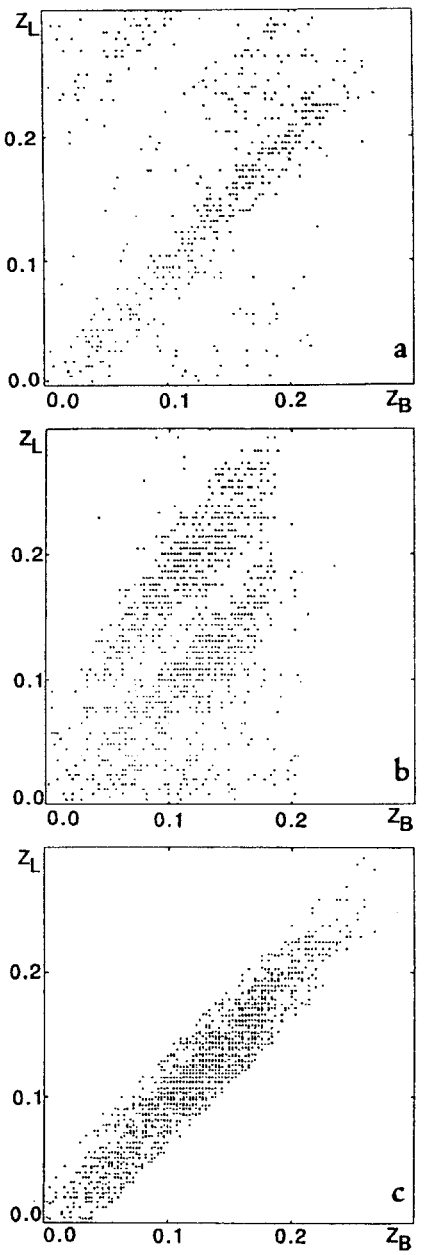

Fig. 7. Redshifts z_L obtained from the least-squares method vs. redshifts z_B obtained from direct break identifications.
7a: One break galaxies
7b: Two break galaxies
7c: z_L-redshifts corrected for false acquisition errors.

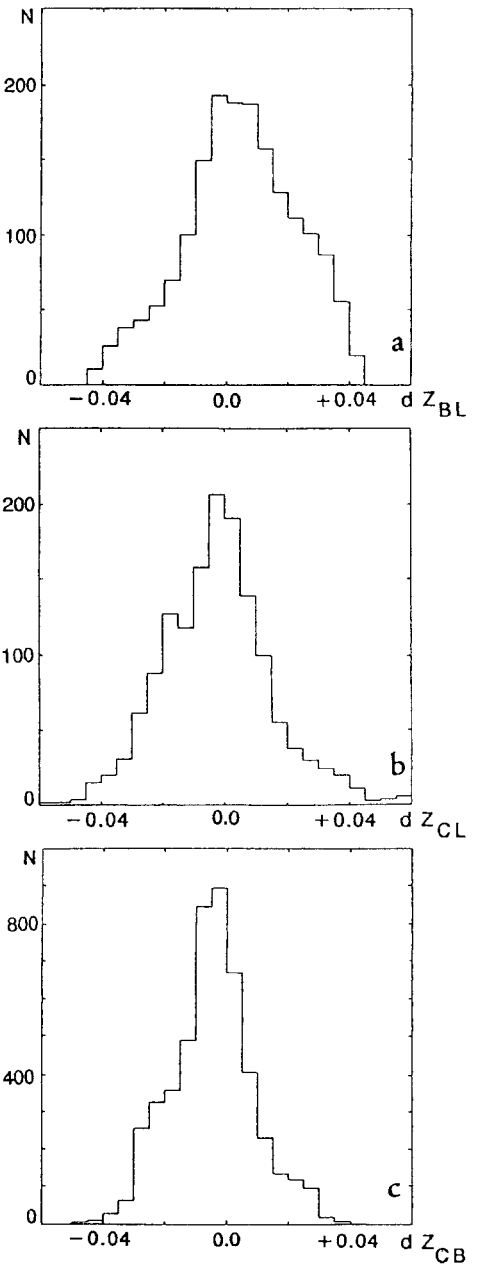

Fig. 8. Histograms of the redshift differences.
8a: dz_{BL}
8b: dz_{CL}
8c: dz_{CB}
The z_L-redshifts are corrected for false acquisition errors.

Table 1. Errors of the redshift measurement methods

relative errors	mean errors	systematic errors	mean sample redshifts	number of galaxies
$dz_{BL} = 0.0196$	$dz_L = 0.0160$	$\delta z_{BL} = +0.0058$	$\langle z_B \rangle = 0.107$	$N = 1\,766$
$dz_{CL} = 0.0177$	$dz_B = 0.0110$	$\delta z_{CL} = -0.0025$	$\langle z_C \rangle = 0.125$	$N = 1\,452$
$dz_{CB} = 0.0135$	$dz_C = 0.0074$	$\delta z_{CB} = -0.0046$	$\langle z_L \rangle = 0.112$	$N = 4\,945$

For each galaxy the averaged redshift $z_0 = \frac{z_L + z_B}{2}$, or $z_0 = z_B$ or z_L when only one reliable redshift could be measured, determines the central value for the redshift range $z_0 \pm \delta z$ where the redshift from the correlation method z_C should be looked for. δz is chosen according to empirical values.

4.2 Statistical errors

In the next step the distributions of redshift differences are used to compute the *statistical* errors of the individual methods dz_B, dz_L, dz_C. If z_T is the true (unknown) galaxy redshift, error differences are given by the equations:

$$\begin{aligned} dz_{BL} &= z_B - z_L = (z_T + dz_B) - (z_T + dz_L) = dz_B - dz_L \\ dz_{CL} &= z_C - z_L = (z_T + dz_C) - (z_T + dz_L) = dz_C - dz_L \\ dz_{CB} &= z_C - z_B = (z_T + dz_C) - (z_T + dz_B) = dz_C - dz_B \,. \end{aligned} \tag{13}$$

dz_{BL}, dz_{CL} and dz_{CB} are obtained from the redshift measurements.

In order to get reliable estimates of dz_L, dz_B and dz_C, variances are calculated. They contain cross terms $\sum dz_i \cdot dz_j$ corresponding to correlated redshift differences dz_i, dz_j:

$$\begin{aligned} dz_{BL}^2 &= dz_B^2 + dz_L^2 - 2 \sum dz_B \cdot dz_L \\ dz_{CL}^2 &= dz_C^2 + dz_C^2 - 2 \sum dz_C \cdot dz_L \\ dz_{CB}^2 &= dz_C^2 + dz_B^2 - 2 \sum dz_C \cdot dz_B \,. \end{aligned} \tag{14}$$

Eqns. 14 show that correlated redshift differences $dz_i \cdot dz_j > 0$ reduce the variances dz_{ij}^2 whereas anticorrelated differences $dz_i \cdot dz_j < 0$ increase them. For statistically independent redshift differences the cross terms vanish leading to a set of equations where the measured variances dz_{ij}^2 uniquely determine the standard deviations of the individual methods.

Table 1 contains the redshift errors of the individual methods obtained from the relative errors. The mean redshift differences δz_{BL}, δz_{CL}, δz_{CB}, the mean redshifts $\langle z_L \rangle$, $\langle z_B \rangle$, $\langle z_C \rangle$ and the numbers N of the galaxies used for the computations are also given. The distributions of dz_{BL}, dz_{CL} and dz_{CB} are shown in *Fig. 8*.

The computations of the individual errors are in general agreement with values derived by Cooke *et al.* (1977, 1981) and Beard *et al.* (1986) for interactive redshift measurements using visual break identifications.

The correlation method is the most accurate redshift measurement technique whereas the least-squares method has the lowest accuracy. This is partially caused by the fact that the correlation method matches *spectral features* while the least-squares method uses the *whole* of the spectrum profiles.

Another reason is that for the correlation method a preset redshift interval $z_0 \pm 0.03$ ties the results to one or both of the redshifts determined by the other methods. With the redshifts not being independent, the corresponding *relative errors* are smaller and so are the resulting *individual errors*. The break measurement technique gives intermediate accuracies: the break measurements are more affected by noise than the correlation measurements.

The systematic differences between the redshifts (δz_{ij}) are small relative to the standard deviations dz_i so that they are presently neglected.

The number of galaxies used for error calculations are different for the individual methods. Most galaxy redshifts are obtained with the break measurement and correlation method. The least-squares method needs the spectral continuum and, therefore, gives reliable redshifts only for the brighter galaxies. This is supported by the computed mean redshifts $\langle z \rangle$ which are lower for the least-squares method.

5 Conclusions and future plans

In Sects. 2 and 3 the automated preprocessing and redshift measurement algorithms used in MRSP were described. Traditional reduction techniques like spectrophotometry, wavelength calibrations, correlation and least-squares methods and new algorithms of pattern recognition, like fuzzy algebra, were applied. The calculated redshift errors of the individual methods are about $dz = 0.01$, corresponding to 3 000 km s^{-1} for single redshift measurements and 0.008, coresponding to 2 300 km s^{-1} for the mean from the two independent redshifts, *e.g.* 25 % of all quoted measurements.

With the method described here it is possible to obtain about 6 000 galaxy redshifts from one objective prism plate at high galactic latitudes for objects with $m_J < 20$. So far, four plates (ESO/SRC fields Nos. 351, 411, 412 and 474) covering more than 100 square degrees, were analyzed. A total number of 200 000 spectra, stellar and non-stellar, were processed. The number of redshifts obtained is 24 000. The accuracies of redshift determinations have since been improved so that now more than 75 % of them are found from two independent methods. By the end of 1988 twelve or more objective prism plates will have been measured with more than 600 000 spectra and more than 70 000 redshifts. With the reduction time of one week per spectral plate (one template), progress is mainly limited by the supply of objective prism plates. Astronomical and cosmological interpretations of the data from field No. 411 are given by Schuecker *et al.* (1988b, c), Schuecker (1988), and Ott (1988).

Acknowledgements

This work is supported by the Deutsche Forschungsgemeinschaft. I especially thank the staff of the UKSTU Edinburgh for the film copies of the objective prism plates.

References

ADAS, 1987. *ADAS Manual*, ed. Teuber, D., Astr. Inst. Univ. Muenster.

Baum, W.A., 1962. In *IAU Symposium No. 15, Problems of Extra-Galactic Research*, ed. McVittie, G.C., Macmillan, New York, p. 390.

Beard, S.M., Cooke, J.A., Emerson, D., MacGillivray, H.T., Kelly, B.D., 1986, *Mon. Not. R. astr. Soc.*, **219**, 251.

Bracewell, R.N., 1978. *The Fourier Transform and its Applications*, McGraw-Hill, Tokyo, p. 46.

Bunclark, P., 1984. *PhD thesis*, Univ. Cambridge, UK.

Clowes, R.G., Emerson, D., Smith, M.G., Wallace, P.T., Cannon, R.D., Savage, A., Boksenberg, A., 1980. *Mon. Not. R. astr. Soc.*, **193**, 415.

Cooke, J.A., Beard, S.M., Emerson, D., 1984. In *IAU Coll. 78, Astronomy with Schmidt-type Telescopes*, ed. Capaccioli, M., Reidel, Dordrecht, p. 401.

Cooke, J.A., Emerson, D., Nandy, K., Reddish, V.C., Smith, M.G., 1977. *Mon. Not. R. astr. Soc.*, **178**, 687.

Cooke, J.A., Emerson, D., Kelly, B.D., MacGillivray, H.T., Dood, R.J., 1981. *Mon. Not. R. astr. Soc.*, **196**, 397.

Cooke, J.A., Emerson, D., Kelly, B.D., 1983. *Workshop on Astronomical Measuring Machines 1982*, eds. Stobie, R.S., MacInnes, B., Royal Observatory Edinburgh, p. 209.

Emerson, D., 1981. *Simulations of UK Schmidt objective prism spectra II: Stars*, Internal Report, Univ. Edinburgh.

Emerson, D., 1983. *Simulations of UK Schmidt objective prism spectra III : Elliptical Galaxies*, Internal Report, Univ. Edinburgh.

Horstmann, H., 1988. *These proceedings*, p. 111.

Humason, M.L., Mayall, N.U., Sandage, A.R., 1956. *Astr. J.*, **61**, 97.

Kurucz, R.L., 1979. *Astrophys. J. Suppl.*, 40, 1.

Loh, E.D., 1988. *These proceedings*, p. 267.

Nandy, K., Reddish, V.C., Tritton, K.P., Cooke, J.A., Emerson, D., 1977. *Mon. Not. R. astr. Soc.*, **178**, 63p.

Oke, J.B., 1971. *Astrophys. J.*, **170**, 193.

Ott., H.-A., 1988. *These proceedings*, p. 274.

Pal, S.K., Dutta Majumder, D.K., 1986. *Fuzzy Mathematical Approach to Pattern Recognition*, Wiley Eastern Limited, New Delhi.

Parker, Q.A., Beard, S.M., MacGillivray, H.T., 1987. *Astr. Astrophys.*, **173**, L5.

Parker, Q.A., MacGillivray, H.T., Hill, P.W., Dodd, R.J., 1986. *Mon. Not. R. astr. Soc.*, **220**, 901.

Ryan, T.W., Hunt, B.R., 1981. In *Progress in Pattern Recognition*, **1**, eds. Kanal, L.N., Rosenfeld, A., North-Holland, Amsterdam, p. 265.

Schuecker, P., 1986a. *Mitt. astr. Ges.*, **65**, 251.

Schuecker, P., 1986b. *Mitt. astr. Ges.*, **65**, 192.

Schuecker, P., 1988. *These proceedings*, p. 160.

Schuecker, P., Horstmann, H., Teuber, D., 1988a. *Proc. Klassifikation und Ordnung*, in press.

Schuecker, P., Horstmann, H., Seitter, W., 1988b. *IAU Symp. No. 130, The Structure of the Universe*, eds. Audouze, J., Szalay, A., Kluwer, Dordrecht, in press.

Schuecker, P., Ott, H.-A., Horstmann, H., Gericke, V., Seitter, W., 1988c. *3rd ESO-CERN Conf. on Cosmology*, Kluwer, Dordrecht, in press.

Schuecker, P., Horstmann, H., Volkmer, C.C., 1986. *Proc. 2nd Workshop on Data Analysis in Astronomy*, eds. Di Gesu, V., Scarsi, L., Crane, P., Friedman, J.H., Levialdi, S., Plenum

Press, New York and London, p. 109.
Seitter, W.C., 1988. In *IAU Workshop Astrophotography*, ed. Marx, S., Springer-Verlag, Berlin, p. 169.
Simkin, S.M., 1974. *Astr. Astrophys.*, **31**, 129.
Teuber, D., 1988. *These proceedings*, p. 323.
Tonry, J., Davis, M., 1979. *Astr. J.*, **84**, 1511.
Tritton, S., 1983. *UKSTU Handbook*, Royal Observatory Edinburgh.
Tucholke, H.-J., 1988. *These proceedings*, p. 136.
Tucholke, H.-J., Schuecker, P., Horstmann, H., Seitter, W.C., 1988. In *IAU Coll. 100, Fundamentals of Astrometry, Celest. Mech.*, eds. Eichhorn, H., Pakvor, I., in press.
West, R.M., Frandsen, S., 1981. *Astr. Astrophys. Suppl.*, **44**, 329.
Zadeh, L.A., 1965. *Inform. and Control*, **8**, 338.
Zadeh, L.A., 1968. *Inform. and Control*, **12**, 94.
Zadeh, L.A., 1973. *IEEE Trans.*, **SMC-3**, 28.
Zadeh, L.A., 1975. In *Fuzzy Sets and Their Applications to Cognitive and Decision Processes*, eds. Zadeh, L.A., Fu, K.S., Tanaka, K., Shimura, M., Academic Press, London, p. 1.